Available online at www.sciencedirect.com
SCIENCE DIRECT®
Journal of Sound and Vibration 279 (2005) 641–667
JOURNAL OF SOUND AND VIBRATION
www.elsevier.com/locate/jsvi

A flexibility-based continuum damage identification approach

L.T. Stutz, D.A. Castello, F.A. Rochinha*

Solid Mechanics Laboratory, Mechanical Engineering Department, Federal University of Rio the Janeiro, P.O. Box 68503, Rio de Janeiro RJ 21945-970, Brazil

Received 17 October 2002; accepted 12 November 2003

Abstract

The present work presents a flexibility-based continuum damage identification approach. Here, it is considered that the current integrity state of a structure is described by means of a continuum damage model. This model enables one to parameterize the stiffness matrix of the finite element (*FE*) model of the system, such that, in an updating process, properties such as symmetry and sparsity of the original *FE* model are naturally preserved. The damage identification is accomplished by minimizing the Frobenius norm of the difference between the experimental and analytical flexibility matrix only related to the measured degrees of freedom (*DOF*) of the structure. By utilizing an error only related to the measured *DOF* one avoids the need for model expansion or model reduction, difficulties commonly present in the model updating process. The modal information required for the experimental flexibility matrix calculation are obtained by means of Eigensystem Realization Algorithm (*ERA*) and common-based structure identification (*CBSI*). The assessment of the present approach has been performed by means of simulations on a beam-like structure considering typical shortcomings occurring in real applications such as small number of sensors, different levels of signal to noise ratio and limited spectral information. It has also been analyzed the use of a regularization term in the error function to be minimized, in order to improve the performance of the proposed method.

1. Introduction

Fracture of components, recognized as a major failure mechanism in structural systems, occurs through three sequential stages: crack initiation, crack growth and final fracture. In the first one, microstructural damage is accumulated leading to a macroscopic crack. The second stage consists

*Corresponding author. Tel.: +55-21-2562-8384; fax: +55-21-2562-8383.
E-mail addresses: stutz@mecsol.ufrj.br (L.T. Stutz), castello@mecsol.ufrj.br (D.A. Castello), faro@serv.com.ufrj.br (F.A. Rochinha).

0022-460X/$ - see front matter © 2004 Elsevier Ltd. All rights reserved.
doi:10.1016/j.jsv.2003.11.043

on a stable growth of this crack contrasting with the third part of the process which often exhibits a dramatic dynamical growth of the failure.

This works as a motivation for the development of very elaborated modelling in order to provide the needed basis for designing safe structural systems. Traditionally, one of the first two stages of the damage process is the focus of the design. On the other hand, there is a new trend, often referred to as damage tolerant approach, which assumes that existence of defects or micro and macro cracks is unavoidable and uses an initial damage scenario to predict the residual life of the system. In both cases, damage identification can play a crucial role. In the most traditional approach, a conciliation between tests, involving laboratories results or in situ data, and the model's response is required in order to achieve reliability. The second approach is to built on the knowledge of the initial damage distribution.

Even when it is not directly connected to design or forecasting, damage identification is a very effective engineering tool as it provides information for maintenance and repairing.

It seems to be widely accepted that damage diagnoses can accomplish four different levels ordered by their complexity, namely: Level 1—detection of damage existence in the structure; Level 2—Level 1 plus determination of damage localization; Level 3—Level 2 plus evaluation of damage intensity; and Level 4—Level 3 plus estimation of the residual life of the structure.

The technological and scientific challenges posed by the different levels above have led to a myriad of approaches aiming at damage identification. Those approaches, encompassing deterministic or statistical perspectives, use different types of data (modal, time series, frequency responses), several forms of excitations and experimental set-ups and distinct mathematical formulations and numerical algorithms. Most prior work on structure damage detection is focused on the general framework of finite element (*FE*) model updating methods. These methods are intended to identify structural damage through determining changes in the physical properties that minimize an error function regarding an undamaged finite element model and experimental data. Very often they rely on the damaged structure's modal parameters (frequencies, mode-shapes and modal damping) exploiting that they are functions of the structural properties (mass, stiffness and damping). Therefore, changes in the physical properties due to damage will be reflected in the modal ones, which can be measured by standard tests and used to infer damage. The technical literature concerning damage identification is very extensive [1–8], and [9] to cite only a few. It is worth mentioning that modern non-destructive damage identification techniques are not completely qualified which implies that they have not been so far fully accepted by the industry and regulatory agencies as practicable methods. This motivates further investigations and improvements of damage identification methods.

Basically, there are three classical damage identification approaches based on *FE* Model Updating, namely: *Optimal Matrix Update* [10,11], *Sensitivity-Based Matrix Update* [12,13] and *Eigenstructure Assignment* [14,15].

The adequacy and performance of using modal data for damage identification is still a controversial issue [7], although this type of approach is very popular in the vibration engineering community. The authors have their own experience on the subject which is reported in Ref. [13], where a combination of dynamical residues involving modal data and a continuum damage model [16] leading to an identification technique is successfully proposed for a number of situations. The technical literature concerning damage identification is very extensive and it presents many other approaches to the problem of damage identification. These approaches encompass, for instance,

the time-domain based methods, which most of them have been developed from control theory and process automation [7,8].

In the present work, a new method based on a continuum damage model as well as on the sensitivity philosophy, which will be referred as Flexibility-based continuum damage identification approach (*FCDIA*) [17] is introduced. This method presents an internal variable that continuously describes the damage experienced by a structure. The updating procedure is built on a constrained minimization of an error measure defined as the square of the Frobenius norm of the difference between the flexibility matrix obtained from a modal test and the analytical flexibility matrix only related to the measured *DOF* of the structure [18,19]. This leads to a nonlinear optimization problem with constraints which is numerically solved through a Newton like method. The connectivity and sparsity of the *FE* original model are naturally preserved. By utilizing an error measure based upon the flexibility matrices, some difficulties commonly present at a model updating are avoided. These difficulties include the necessity of a modal expansion technique or a modal reduction to the dimension of the measured *DOF* and the selection of the modes that will be used in the adjustment procedure, once an accurate estimate of the experimental flexibility matrix may be obtained from a few of the lower frequency modes.

The proposed identification technique is grounded in a physically parameterized *FE* model [20] which, in contrast to statistical analysis of time series [21], entails shortcomings like the introduction of uncertainties associated with the discretization errors or modelling errors. The motivation for employing such approach relies on its utility as mechanism, at least ideally, for improving the knowledge of the physics of damage processes which, in turn, enlarges the predictive ability concerning the remaining life of the structure and helps on the future modelling and on the design optimization of similar systems. Furthermore, once the damage model is improved and validated by a technique like the *FCDIA*, it could be used to supply training data for on line autonomous health monitoring based on pattern recognition or on neural networks.

In order to shed some light on the use of the flexibility matrix in the proposed damage detection method, the sensitivity of the modal data related to a single spring mass model of a structure is analyzed. The system's natural frequency is related to the stiffness k and mass m by $w_n = \sqrt{k/m}$. Considering that only the stiffness is affected by the damage, the natural frequency of the damaged system is given by $w_n^D = \sqrt{k\beta/m}$, where β, an indicator of the structural defect that will be detailed later, varies between 0 (totally damaged structure) and 1 (healthy structure). Therefore, the relative sensitivity of the natural frequency to changes in the stiffness due to damage reads as

$$\frac{\mathrm{d}}{\mathrm{d}\beta}\left(\frac{w_n^D}{w_n}\right) = \frac{1}{(2\sqrt{\beta})}.$$

On the other hand, the flexibility matrix G, which reduces to $1/k$ into this one degree of freedom setting, presents the following sensitivity to damage:

$$\frac{\mathrm{d}}{\mathrm{d}\beta}\left(\frac{\mathrm{g}^D}{g}\right) = \frac{-1}{\beta^2}.$$

Sensitivity is a key point in any identification process, so, from that perspective, one could conclude that the flexibility is a better damage indicator as its sensitivity to damage is significantly

larger than the natural frequency's one. That means that the former is more affected by the presence of a defect, which can improve the conditions of detecting it.

The introduction of a continuum damage model makes it possible to follow the degradation process from its very beginning till the onset of the nucleation of a macro crack evolved from the microdefects represented through the damage field β. Therefore, assuming that damage behaves isotropically in this initiation phase, which means that closure of micro cracks during compression are not taken into account, the *FCDIA* is intended to identify flaws in their early stages. It is worth mentioning that the damage modelling remains valid in the presence of a macro crack, but *FCDIA*, which relies on the linear dynamic response of the structure, is no longer effective.

Damage identification fits in the broad category of inverse problems [7,22], which are normally ill-posed. That means, for instance, that two or more different damage scenarios, or even none, could correspond to the same measured structural response which provides the basis for the sought identification. Inverse problems are also very difficult to be handled by numerical algorithms, as they lead to ill-conditioned mathematical formulations. In order to circumvent those difficulties in implementing the proposed damage identification technique a regularization method [23,24] was adopted. This method, known as Thikonov regularization, introduces a new functional to be minimized by adding to the former one a quadratic term involving a norm of the sought solution. This method establishes a balance between conciliating the measured data with the model and to retrieve a priori desired or known features of the identified parameters. Here, the L_2 norm of the damage parameter gradient is taken as the regularization term.

The remainder of the paper is organized as follows. Section 2 presents the theoretical aspects of the proposed method, comprising a presentation of the basic involved quantities and the principles of the continuum damage model to be used in the *FCDIA*. Section 3 presents the numerical details of the Newton's Method applied to the present problem. Finally, Section 4 presents some illustrative examples to assess the main characteristics of *FCDIA*, where some of the simulations of the damage identification have been performed on a cantilever beam through a virtual test simulator. This simulator was used in order to provide a more realistic character to the simulations. A special attention is devoted to the role played by the regularization method mentioned beforehand.

2. Theoretical background

This section is devoted to present the fundamentals of the model based damage identification technique to be introduced . As structures are modelled as distributed parameter systems, the first step on building such technique relies on obtaining a discrete version of the model. Here the finite element method is adopted due to its recognized efficiency on dealing with structural systems.

The stiffness and flexibility matrices $\mathbf{K}$ and $\mathbf{G}$ of an undamped *n-DOF* finite element model of a structural system can be represented as functions of the system modal parameters as follows:

$$\mathbf{K} = \mathbf{M}\boldsymbol{\Phi}\boldsymbol{\Omega}\boldsymbol{\Phi}^{\mathrm{T}}\mathbf{M} = \mathbf{M}\left(\sum_{i=1}^{n} \omega_i^2 \phi^{(i)} \otimes \phi^{(i)}\right)\mathbf{M}, \tag{1}$$

$$\mathbf{G} = \mathbf{\Phi}\mathbf{\Omega}^{-1}\mathbf{\Phi} = \sum_{i=1}^{n} \frac{1}{\omega_i^2}\phi^{(i)} \otimes \phi^{(i)}, \tag{2}$$

where $\mathbf{M}$ is the system mass matrix, $\mathbf{\Phi} = [\phi^{(1)} \ldots \phi^{(n)}]$ is the mass-normalized mode shape matrix, $\phi^{(i)}$ is the ith mass-normalized mode shape, $\mathbf{\Omega} = \text{diag}\{\omega_1^2 \ldots \omega_n^2\}$ is a diagonal matrix containing the square of the system natural frequencies and $\otimes$ denotes the tensor product.

As one can see from Eq. (1), the higher the frequency, the greater the modal contribution to the stiffness matrix. Hence, in order to obtain an accurate estimate of the experimental stiffness matrix all the modal properties are required, or at least the ones associated with the higher frequencies. However, in practice, due to experimental limitations, only a few of the lower modes can be measured.

On the other hand, as one can see from Eq. (2), the higher the frequency, the smaller the modal contribution to the flexibility matrix. Hence, a good estimate of the flexibility matrix can be obtained from a few of the lower frequency modes. This characteristic of the flexibility matrix leads to its fast convergence with increasing values of frequency. Although only a few of the lower frequency mode shapes are necessary for a good estimate of the flexibility matrix, all of them must be full-*DOF* mode shapes. Nevertheless, in practice, the number of *DOF* at which the mode shapes are sampled is typically much smaller than the number of *DOF* of the *FE* model. As a straightforward result, the experimental measured flexibility matrix $\mathbf{G}_E$ is not computed for the full-*DOF* set, but only for the instrumented ones, i.e.

$$\mathbf{G}_E = \sum_{i=1}^{n_E} \frac{1}{\omega_{i,E}^2}\phi_E^{(i)} \otimes \phi_E^{(i)}, \tag{3}$$

where $n_E < n$ is the number of modes computed from modal testing, the subscript E refers to an experimental property and $\phi_E^{(i)}$ corresponds to the ith experimental mode shape.

It should be noticed from Eq. (3) that the number of experimental modes n_E does not influence the dimension of the experimental flexibility matrix $\mathbf{G}_E$, which depends only on the number of measured *DOF*. Hence, if only m *DOF* are measured in the modal testing, the mode shapes will have dimension $m \times 1$, leading to an $m \times m$ experimental flexibility matrix. One should remark that this $m \times m$ matrix does not have any relation to the inverse of any $m \times m$ partition of the stiffness matrix.

Aiming at obtaining a relation between the experimental flexibility matrix $\mathbf{G}_E$ and an $m \times m$ matrix which contains information about stiffness properties of the structure, the original stiffness matrix $\mathbf{K}$ should be reorganized according to the measured *DOF*. Partitioning the n *DOF* of the system into the m measured *DOF* and the o omitted ones, the ith mode shape is as follows:

$$\phi^{(i)} = \begin{Bmatrix} \phi_m^{(i)} \\ \hline \phi_o^{(i)} \end{Bmatrix}. \tag{4}$$

According to this partition of *DOF*, the flexibility and stiffness matrices are partitioned as

$$\mathbf{G} = \begin{bmatrix} \mathbf{G}_{mm} & \mathbf{G}_{mo} \\ \mathbf{G}_{mo}^{\mathrm{T}} & \mathbf{G}_{oo} \end{bmatrix}, \quad \mathbf{K} = \begin{bmatrix} \mathbf{K}_{mm} & \mathbf{K}_{mo} \\ \mathbf{K}_{mo}^{\mathrm{T}} & \mathbf{K}_{oo} \end{bmatrix}. \tag{5, 6}$$

It can be shown [25] that the inverse of the analytical flexibility matrix related to the measured *DOF* is equal to the Guyan-reduced (or statically condensed) system stiffness matrix $\bar{\mathbf{K}}$ [26] with respect to the same set of *DOF*, viz.

$$\mathbf{G}_{mm} = \bar{\mathbf{K}}^{-1} = [\mathbf{K}_{mm} - \mathbf{K}_{mo}\mathbf{K}_{oo}^{-1}\mathbf{K}_{mo}^{\mathrm{T}}]^{-1}. \tag{7}$$

Hence, as it has been shown in Eq. (7), changes in the modal properties based on the flexibility matrix, reflected by changes in the stiffness matrix, may be used, at least in principle, for damage detection, location and extent determination.

2.1. Continuum damage model

Continuum damage mechanics describes in a unified fashion the two first stages of fracture. Therefore it seems to be very convenient to link it to damage identification, which has motivated the authors to explore this combination using two different approaches [8,13], other than the one proposed here.

Along with classical variables that characterize the kinematics of a continuum medium (displacements and velocities of material points labelled as $\mathbf{x}$), an additional scalar variable $\beta \in [0, 1]$ is introduced. This variable is related to the links among material points and can be interpreted as a measure of the local cohesion state of the material. This field of cohesion states describes the current state of damage within the mechanical system as it evolves in time and possesses as extreme values $\beta = 0$ and 1. Therefore, if at a certain time t, after a period of evolution of the system, $\beta = 1$, all the links and the initial material properties have been preserved. On the other hand, if $\beta = 0$ a local rupture is considered since all the links among material points have been broken. The variable β is associated to the damage variable D, [27], by the following relation: $\beta = 1 - D$. As the degradation is an irreversible phenomenon, the rate $\dot{\beta}$ must be negative or equal to zero. Summarizing, D is a macroscopic field variable which represents microstructural material damage in an average sense. It is treated as an internal variable that appears in the constitutive relation, thus taking into account the degradation on the material's mechanical properties. A detailed presentation of the basic principles that govern the evolution of such kind of continuum damage can be found in Refs. [16,28].

Due to the fact that the goal of the present work is damage identification, it is considered that the damage does not evolve during the dynamic tests, i.e., $\dot{\beta} = 0$. In other words, it is supposed that the level of internal forces in the structure during the experiment does not suffice to cause the continuation of the damage process, implying that β is only a function of the spatial variable $\mathbf{x}$.

The modelling considers that only the elastic terms contained in its basic equations are affected by the damage field. Thus, the components of the stiffness matrix obtained by a spatial discretization using the finite element model read as

$$K(\beta_h)_{ij} = \int_{\Omega} \beta_h(\mathbf{x})[\mathbf{D}^{\mathrm{T}}\mathbf{E}\mathbf{D}]_{ij}(\mathbf{x})\,\mathrm{d}\Omega, \quad i,j = 1, \ldots, 3m_h, \tag{8}$$

where $[\mathbf{D}]$ denotes the standard discretized differential operator, $[\mathbf{E}]$ is the matrix of the elastic constitutive coefficients, m_h is the number of nodal points related to the finite element discretization and β_h is the approximation for the damage field.

As the damage is described exclusively by the variable β, which is continuously defined over the whole elastic continuum body, the severity of the damage can be differentiated within the elements of the structure. This method differs from the classical ones in which the damage is associated with a classical parameter of the structure, such as Young modulus E, and the damage is not supposed to affect the stiffness properties of adjacent elements. Therefore, the capability of the present method to represent the damage of the structure is greatly supported by the discretization β_h of the damage field, which is not necessarily coincident with the one used for the displacement field. As an example, the elemental stiffness matrix $[\mathbf{k}^e]$ of the C^1 Euler–Bernouilli beam element assuming the damage field interpolated using linear classical Lagrangian piecewise linear shape functions reads as

$$\frac{8h^3}{EI}\mathbf{k}^{(e)} = \begin{bmatrix} 36\beta_i + 24\beta_q + 36\beta_j & 2h(13\beta_i + 6\beta_q + 5\beta_j) & -36\beta_i - 24\beta_q - 36\beta_j & 2h(5\beta_i + 6\beta_q + 13\beta_j) \\ 2h(13\beta_i + 6\beta_q + 5\beta_j) & h^2(19\beta_i + 10\beta_q + 3\beta_j) & -2h(13\beta_i + 6\beta_q + 5\beta_j) & h^2(7\beta_i + 2\beta_q + 7\beta_j) \\ -36\beta_i - 24\beta_q - 36\beta_j & -2h(13\beta_i + 6\beta_q + 5\beta_j) & 36\beta_i + 24\beta_q + 36\beta_j & -2h(5\beta_i + 6\beta_q + 13\beta_j) \\ 2h(5\beta_i + 6\beta_q + 13\beta_j) & h^2(7\beta_i + 2\beta_q + 7\beta_j) & -2h(5\beta_i + 6\beta_q + 13\beta_j) & h^2(3\beta_i + 10\beta_q + 19\beta_j) \end{bmatrix}, \tag{9}$$

where h is length of the element, I is the moment of inertia, A is the cross-sectional area, β_i and β_j are the nodal cohesion parameters associated with the nodes i and j of the element of the FE mesh of the displacement field, and β_q is the nodal cohesion parameter associated to an intermediate node placed in the middle of each element of the displacement's mesh. The derivation of the above equation is presented in Ref. [13].

The convenience of having two different discretizations for the damage and displacement fields is demonstrated in the examples presented later on.

3. Identification problem

Aiming at the damage identification, it is assumed that the FE model is reliable and that eventual discrepancies found between analytical and experimental information is mainly due to the presence of damage in the structure. Key issues concerning uncertainties are not addressed here. Uncertainty may be introduced in the identification process due to lack of information about the involved parameters or to the unavoidable noise contained in the obtained data. The aforementioned parameters are not only those related to materials characteristics but also those linked to the discretization process. In order to handle that source of uncertainty, one could add a previous step consisting of updating the FE model of the healthy structure to the proposed methodology. The numerical results presented later will demonstrate that damage identification is achieved by $FCDIA$ even when noisy data is used.

The inverse damage identification problem is now posed as a finite dimensional optimization formulation that reads as follows.

Find $\mathbf{B} = \{\beta_1, \ldots, \beta_{n_d}\}^{\mathrm{T}}$, a minimum of

$$J(\mathbf{B}) = \tfrac{1}{2}\|\mathbf{G}_{mm} - \mathbf{G}_E\|_F^2 = \tfrac{1}{2}[\mathbf{G}_{mm} - \mathbf{G}_E] : [\mathbf{G}_{mm} - \mathbf{G}_E]$$
$$\text{such that } \beta_j \in [0,1], \quad j = 1, \ldots, n_d, \tag{10}$$

where $\|\cdot\|_F$ stands for the Frobenius norm and : denotes the matrix scalar product. Vector $\mathbf{B}$ defines the discretized cohesion parameter field. When a Finite Element Method is adopted, $\{\beta_1, \ldots, \beta_{n_d}\}$ are the nodal values of $\beta_h(\mathbf{x})$. The above functional represents a least-square error between measured and model responses of the damaged structure.

It is generally very difficult to obtain an analytical solution to the optimization problem introduced above. Therefore, one has to resort to numerical algorithms that might present poor performance when noisy data is used due to the ill-posedeness of the problem. This is partially circumvented by adopting a regularization method in which a regularization term is added to the error function, which leads to a new functional, viz.

$$J_\alpha(\mathbf{B}) = J(\mathbf{B}) + \alpha f(\mathbf{B}), \tag{11}$$

where α and $f(\mathbf{B})$ are respectively a regularization factor and a regularization function. Here, f is restricted to a discrete version of the β's gradient L^2 norm, which means, broadly speaking, that one is seeking a regular solution. From a physical standpoint, it represents a penalization over damage scenarios corresponding to sharp transitions between damaged and undamaged regions. It is important to note that it does not eliminate such possibility, as it is needed for special cases when damage is very localized. The choice of α was conducted by an heuristic approach by observing the numerical results. This could be improved by using optimized schemes for this choice [24]. Here, the regularization factor α has been chosen based on the stopping criterium adopted for the numerical updating process, viz.

$$\alpha = \alpha_0 = \frac{\varepsilon_0}{10}, \tag{12}$$

where $J < \varepsilon_0$ is one of the criteria that must be satisfied to stop the updating process.

It is important to emphasize that once the nodal vector $\mathbf{B}$ has been determined, the damage value at any point of the body can be reached by using the interpolation functions adopted in the β discretization. Therefore, it is possible to obtain an evaluation of the damage state over the whole elastic structure.

4. Numerical damage determination

This section presents the details of the numerical algorithm, based on the Newton Method, used in the solution of the optimization problem introduced previously. The algorithm fits into the category of sensitivity based methods [12,13,29].

The solution of the problem stated in Eq. (10) consists of the set of the most suitable nodal cohesion parameters $\mathbf{B} = \{\beta_1 \ldots \beta_{n_d}\}^{\mathrm{T}}$ satisfying the following optimality equations:

$$F_j = \frac{\partial J_\alpha}{\partial \beta_j} = 0 \quad \text{satisfying } \beta_j \in [0,1], \quad j = 1, \ldots, n_d, \tag{13}$$

each equation consisting of the first derivative of the scalar function J_α with respect to the jth cohesion parameter.

From Eqs. (11), (10) and (13), one gets

$$F_j = -[\mathbf{G}_E - \mathbf{G}_{mm}] : \frac{\partial \mathbf{G}_{mm}}{\partial \beta_j} + \alpha(\mathbf{RB})_j, \tag{14}$$

where the positive semi-definite matrix $\mathbf{R}$ is defined as

$$\mathbf{R}_{ij} = \int_\Omega [\mathbf{D}^{\mathrm{T}}\mathbf{D}]_{ij}\, \mathrm{d}\Omega$$

and the matrix $\mathbf{D}$ is the same one that appears in Eq. (8). The first derivative of the flexibility matrix with respect to the cohesion parameters can be determined by differentiating the identity

$$\bar{\mathbf{K}}\mathbf{G}_{mm} = \mathbf{I}, \tag{15}$$

where $\mathbf{I}$ is the $m \times m$ identity matrix. Performing a suitable manipulation in Eq. (15) yields

$$\frac{\partial \mathbf{G}_{mm}}{\partial \beta_j} = -\mathbf{G}_{mm}\frac{\partial \bar{\mathbf{K}}}{\partial \beta_j}\mathbf{G}_{mm}. \tag{16}$$

The non-linear system engendered by Eq. (13) is numerically solved by Newton's Method. The constraint of the cohesion parameters is imposed performing a simple projection, such that at the rth iteration the approximation of the cohesion parameter vector reads as

$$\mathbf{B}^{(r)} = \mathbf{S}(\mathbf{B}^{(r-1)} + \Delta\mathbf{B}^{(r)}), \tag{17}$$

where the operator $\mathbf{S}$ is, essentially, a simple projection defined over each component of $\mathbf{B}$ defined as

$$\mathbf{S}(\chi) = \{\chi \text{ if } \chi \in [0,1];\ 1 \text{ if } \chi > 1; 0 \text{ if } \chi < 0\}, \tag{18}$$

where the increment $\Delta\mathbf{B}^{(r)}$ comes from the Newton's iteration

$$\mathbf{A}^{(r-1)}\Delta\mathbf{B}^{(r)} = -\mathbf{F}^{(r-1)}, \tag{19}$$

where the matrix $\mathbf{A}$ represents the tangent matrix of the Newton's Method, whose components are defined as

$$A_{ij} = \frac{\partial F_i}{\partial \beta_j} + \alpha\mathbf{R}_{ij} \tag{20}$$

and are obtained as

$$A_{ij} = \frac{\partial \mathbf{G}_{mm}}{\partial \beta_j} : \frac{\partial \mathbf{G}_{mm}}{\partial \beta_i} - [\mathbf{G}_E - \mathbf{G}_{mm}] : \frac{\partial^2 \mathbf{G}_{mm}}{\partial \beta_i \partial \beta_j} + \alpha\mathbf{R}_{ij}. \tag{21}$$

One should notice that as the flexibility matrix is a function of the cohesion parameters, it must be updated at each iteration. Therefore, after determining matrix $\mathbf{A}$ and the residual vector $\mathbf{F}$ for the rth iteration, the increment $\Delta\mathbf{B}^{(r)}$ is given by

$$\Delta\mathbf{B}^{(r)} = [\mathbf{A}^{(r-1)}]^{-1}\mathbf{F}^{(r-1)}. \tag{22}$$

5. Illustrative examples

Here, the verification and assessment of the current damage identification approach involve an "analytically derived modal test structure". It is based on the two main tasks: the first one consists of imposing some damage to a chosen test structure and performs a virtual modal experiment on it, ignoring the knowledge of both the location and the magnitude of the imposed damage. The second uses *FCDIA* to assess damage considering as entry the dynamic response of the damaged fictitious test model.

The reliability evaluation of the proposed damage identification technique (*FCDIA*) is performed on a cantilever bidimensional Euler–Bernouilli beam. This same structure was used in other damage identification approaches based on the same continuum damage modelling [8,13], that *FCDIA* is built on.

The 1 m cantilever beam comprises 20 bidimensional Euler–Bernouilli beam elements of length $h = 0.05$ m, which leads to a *FE* model containing 40 *DOF* (20 translational, 20 rotational). The beam is depicted in Fig. 1 and its material properties have been chosen as reported in Table 1. Within the frequency band of interest (0–450 Hz), the system contains six modes and the following modal damping ratios were considered: $\zeta_1 = 0.058\%$, $\zeta_2 = 0.508\%$, $\zeta_3 = 0.309\%$, $\zeta_4 = 0.378\%$, $\zeta_5 = 0.500\%$ and $\zeta_6 = 0.400\%$.

In order to realistically simulate the corrupting effects of noise, filtering, digital sampling and truncation of the modal spectrum, a virtual simulator was utilized. The simulator estimates the frequency response function (*FRF*) for each input-output pair through ensemble averaging. In order to achieve a higher level of fidelity, the input signal is pre-filtered before the analog conversion. The noise contaminated system response is the available one to be processed, and this signal is filtered at 80% of the Nyquist frequency before digital sampling. As reported in Ref. [25], this procedure furnishes realism to the *FRF* obtaining problem. The *FRF*s obtained from the virtual simulator are used to derive impulse response functions required for the eigensystem realization algorithm (ERA) [30], which in turn, provides a state-space equation of the structure. The state-space equation derived from this realization is used further in the *CBSI* algorithm [31]

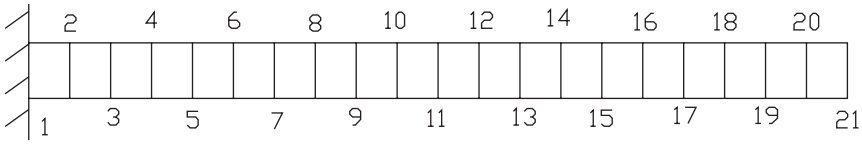

Fig. 1. Cantilever beam (and its *FE* mesh) used to assess *FCDIA*.

Table 1
Material properties of the beam

Young modulus E	69 Gpa
Cross-sectional area A	1.82×10^{-4} m^2
Moment of inertia I	1.46×10^{-9} m^4
Specific mass ρ	6.8×10^{3} kg/m^3

which provides the required normal modal properties, namely, the normal mode-shapes at the measured *DOF* and the natural frequencies.

For the required data acquisition, the excitation point will always be at the first sensor position and the acquisition data parameters shown in Table 2 were adopted. The noise contaminated system response is derived considering the following definition of signal to noise ratio (*SNR*):

$$SNR = 10 \log\left(\frac{\sigma_s^2}{\sigma_n^2}\right), \tag{23}$$

where σ_s^2 and σ_n^2 correspond to the variances of signals s and n respectively.

Although there had been six modes within the frequency band of interest, only the five first ones were used for the updating processes. It helps to illustrate the fact that although not all the available spectral information is required for the updating process, the set of not used information is important in the validation of the damage identification result by inspecting the error measures computed from the entire spectral information.

A number of examples is presented aiming at assessing the influence of noisy data, of reduced measured *DOF*, of the number of samples and averages used in the data acquisition and of the regularization term in the results provided by *FCDIA*. This set of numerical examples is summarized in Table 3. In the first six cases, the *FE* meshes of damage and displacement fields are

Table 2
Data acquisition parameters

Sample frequency	1200 Hz
Number of samples	4096
Test band of interest	0–450 Hz
Excitation type	sine chirp

Table 3
Simulation parameters

Case	*SNR* (dB)	Measured *DOF* (nodes)	Updated parameters	α	Number averages
1	90	2, 4, 6, …, 20	all	α_0	10
2	90	2, 6, 10, 14, 18	all	α_0	10
3	90	2, 6, 10, 14, 18	all	see Fig. 10	10
4	40	2, 6, 10, 14, 18	all	α_0	10
5	40	2, 5, 8, 14, 21	2–9	0	10
6	20	2, 6, 10, 14, 18	all	α_0	100
7[a]	90	2, 4, 6, …, 20	all	α_0	10
8[a]	20	2, 6, 10, 14, 18	all	α_0	100
9[a]	20	2, 5, 8, 14, 21	all	α_0	100
10[a]	20	2, 5, 8, 14, 21	4–11	0	100
11[a]	20	2, 5, 8, 14, 21	5–11	0	100

[a] The number of nodes associated to β_h is the double of the one used in the displacement's mesh.

coincident, consisting of piece-wise linear functions. The damage is spread over the same three elements for all the cases. In cases (7)–(11) there is no mesh coincidence and the damaged zone is completely enclosed within a single element of the *FE* mesh of the displacement field.

In case (1), a linear damage distribution is imposed over elements between nodes 4 and 7 as depicted in Fig. 1.

The damage is defined by its values at nodes 5 (0.20 m) and 6 (0.25 m), in which the variable D was set to be 0.2 and 0.05, respectively, and null values were assumed at all other positions. The vertical components of the first five modes were available at every other node. It has been considered that the signal was polluted with noise such that the signal to noise ratio was $SNR = 90$ dB, which corresponds to a very accurate measure. All the 21 cohesion parameters were allowed to be updated, i.e., no damage location step was first performed, which could indicate the most likely damaged regions and, consequently, allowed only a small number of cohesion parameters to be updated.

Three error measures are adopted in order to evaluate the performance of *FCDIA*. The relative error between the experimental and the analytical natural frequencies E_f, the amplitude correlation coefficient ACC [32] and a normalized global time error measure.

The amplitude correlation coefficient ACC is defined as

$$ACC(\omega) = \frac{2|\mathbf{H}_E(\omega)^H \mathbf{H}(\omega)|}{\mathbf{H}_E(\omega)^H \mathbf{H}_E(\omega) + \mathbf{H}(\omega)^H \mathbf{H}(\omega)}, \tag{24}$$

where $\mathbf{H}(\omega)$ is a vector comprised of all the available *FRF*s at the frequency ω. The ACC is defined between zero and unity, and it only becomes unity if the amplitudes of the *FRF*s coincide.

The normalized global time error GTE is defined as

$$GTE(t) = \sum_{j=1}^{n_s} \frac{Y_{E,j}(t) - Y_{m,j}(t)}{\|Y_{E,j}(t)\|}, \tag{25}$$

where $Y_{E,j}$ and $Y_{m,j}$ correspond to the system response and to the model response respectively, at the jth system sensor, regarding the same excitation and n_s correspond to the number of available sensors.

The result provided by *FCDIA* for case (1) is depicted in Fig. 2. It is clear from this figure that the essence of the damage field was captured by *FCDIA*. However, it should be remarked that the reliability of the provided result must be based on the error indicators computed from the available data. The relative frequency error indicator E_f is depicted in Fig. 3 and it shows that all the model natural frequencies, except the second one, have gotten closer to the experimental natural frequencies. The ACC measure, depicted in Fig. 4, clearly shows a great improvement of the *FRF*s, except at the first natural frequency. Nevertheless, it should be remarked that, within this band, the poor *FRF*s curve fitting, due to precision errors in frequency associated to the Discrete Fourier Transform may be responsible to make the ACC error measure almost invariant within this band. The normalized global time-error GTE also shows a better agreement between the response of the damaged structure and that of the updated model than the response of the original one as can be noted in Fig. 5. Hence, all the error measures are positive with respect to the response provided by the *FCDIA*, i.e., all of them show that damage identification has led to a

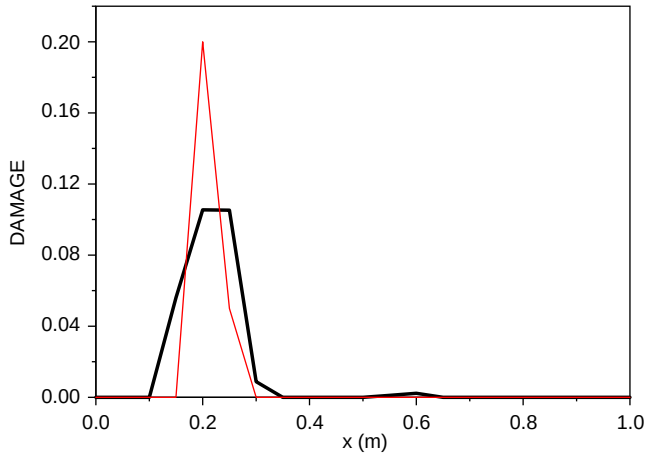

Fig. 2. Result obtained by *FCDIA* for case (1). Thin line: correct; thick line: obtained.

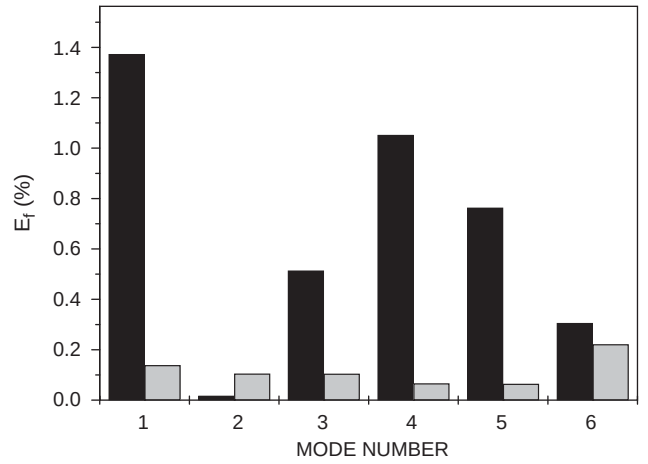

Fig. 3. Relative frequency error indicator E_f for case (1). Black columns: initial; gray columns: final.

better agreement between the updated model and the actual damaged structure, which implies that the result can be considered satisfactory, a fact that agrees with Fig. 2.

The second situation (2) differs from the first one only in the number of sensors. Now only half of the sensors are used, such that measured *DOF*s are the vertical ones corresponding to the nodes 2, 6, 10, 14 and 18. The result provided by *FCDIA* is shown in Fig. 6.

It is clear from Fig. 6 that the present result describes the damage field as well as it has been described in the previous example, for the same algorithm stopping criteria. The error measures associated with the result provided by *FCDIA* for case (2) are depicted in Figs. 7–9. As one can see, when comparing the error measures for cases (1) and (2), it is really difficult to assure that, in this situation, one solution is more consistent than the other one. This fact may be considered as

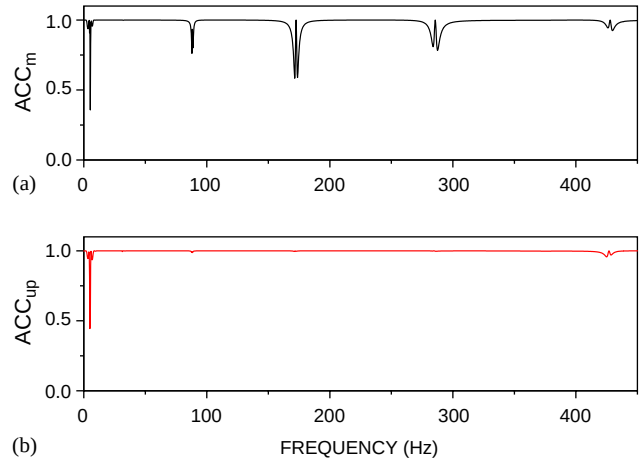

Fig. 4. Amplitude Correlation Coefficient *ACC* for case (1). (a) ACC_m: original model; (b) ACC_{up}: updated model.

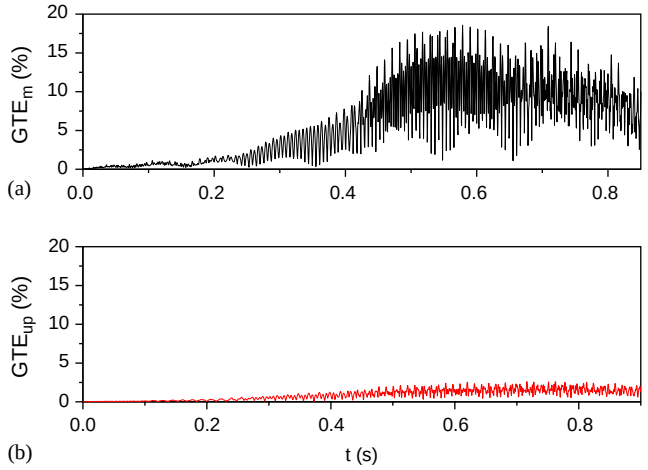

Fig. 5. Normalized global time error *GTE* for case (1). (a) GTE_m: original model; (b) GTE_{up}: updated model.

predictable as long as it is well known that, in several situations, the dynamic behavior of a structure is slightly changed due to damage.

In the third case (3) the influence of the regularization term is considered. Damage identification is performed for different values of the regularization coefficient α. Fig. 10 discloses the importance of the regularization term in the updating process. There one should note that the result provided by *FCDIA* when the regularization coefficient α is equal to zero indicates a second possible solution for the present damage state of the structure. In this false scenario, three damaged regions are indicated. One encompasses the imposed damage region and the other two the region near the fixed and free ends of the beam, where damage does not really exist. This does not sound strange, inasmuch as inverse problems have as a major drawback ill-posedness, which

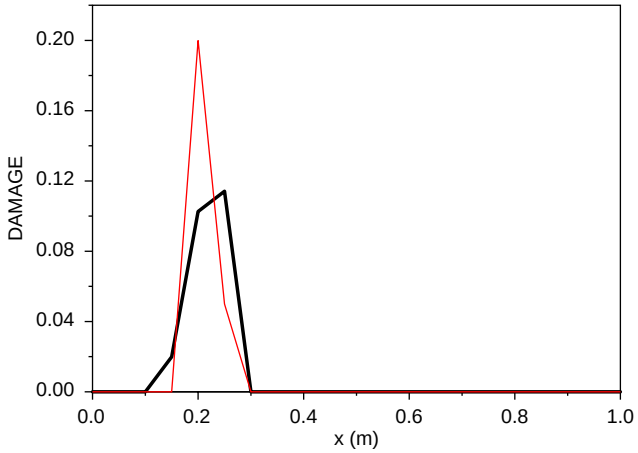

Fig. 6. Result obtained by *FCDIA* for case (2). Thin line: correct; thick line: obtained.

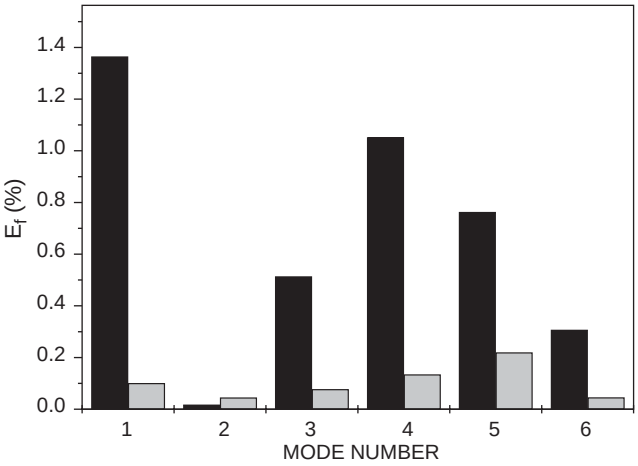

Fig. 7. Relative frequency error indicator E_f for case (2). Black columns: initial; gray columns: final.

might imply the existence of more than one solution [23]. When the regularization coefficient α is made different from zero, all the identified damage regions are in agreement with the really imposed damage. However, as the regularization term imposes a penalty in the gradient of the damage field, the larger the regularization coefficient α the smaller the maximum damage amplitude obtained by *FCDIA*, i.e., the identified damage tends to be smaller in amplitude and greater in its support. That reinforces the need of seeking for an optimal regularization parameter that grants a well-balanced inverse formulation, which leads to a physically meaningful and numerically stable solution.

The fourth case (4) to be analyzed is carried out under the same conditions of case (2), except for the signal to noise ratio *SNR*, which has been set equal to 40 dB. The result provided by

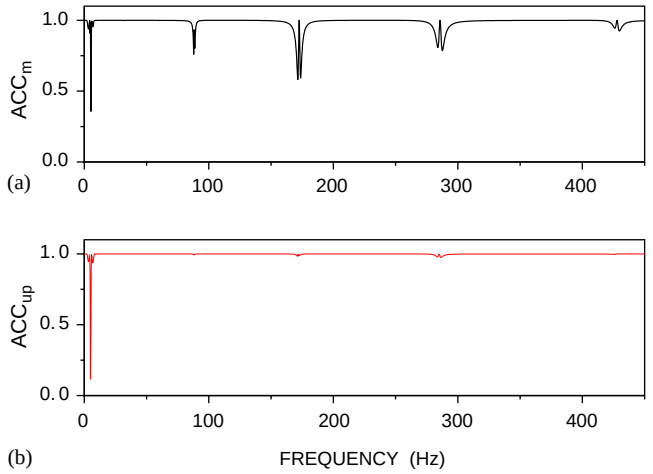

Fig. 8. Amplitude Correlation Coefficient *ACC* for case (2). (a) ACC_m: original model; (b) ACC_{up}: updated model.

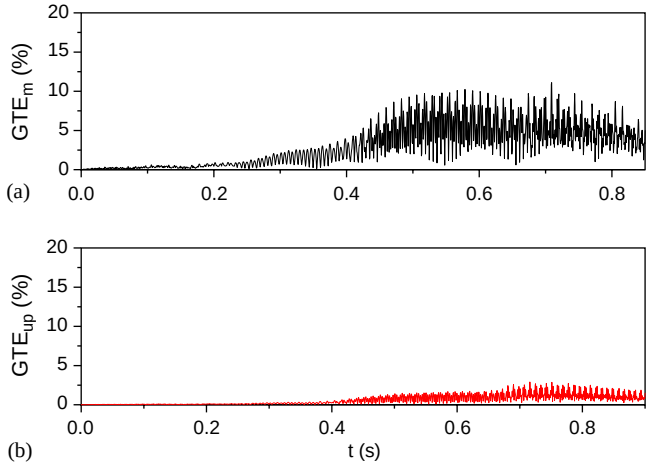

Fig. 9. Normalized global time error *GTE* for case (2). (a) GTE_m: original model; (b) GTE_{up}: updated model.

FCDIA is depicted in Fig. 11. As one can see, despite the presence of more noise in the data, the result depicted in Fig. 11 is approximately the same as that of Fig. 6.

It is well known that after performing an experiment if one decides to do a different one, such as keeping everything the same but the position of sensors, it can be really simple or almost not practical. However, despite the difficulties inherent in this process, a second assessment of the identified damage field can be obtained performing a new experiment, if it is possible. Therefore, the damage identification result depicted in Fig. 11 will be assessed by a new experiment (5). The damaged region pinpointed in Fig. 11 will be considered as the result of a damage location step, which allows one to relocate the sensors to more suitable positions and to choose a small set of cohesion parameters to be updated. Hence, the vertical *DOF*s of the nodes 2, 5, 8, 14 and 21 are

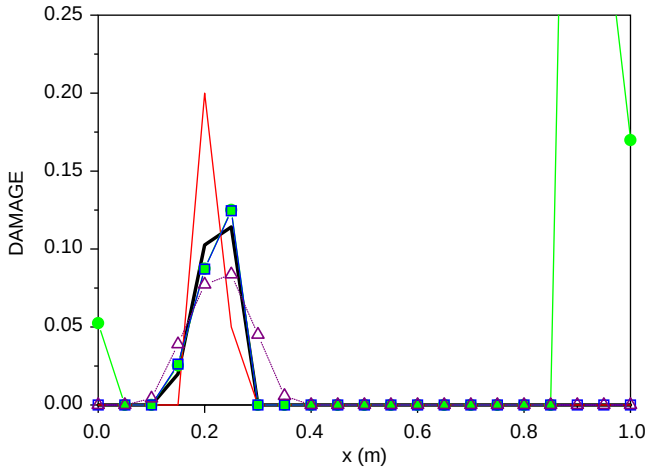

Fig. 10. Result obtained by *FCDIA* for case (3). Thin line: correct; thick line: $\alpha = \alpha_0$, •; $\alpha = 0$, □; $\alpha = 0.01\alpha_0$, △; $\alpha = 100\ \alpha_0$.

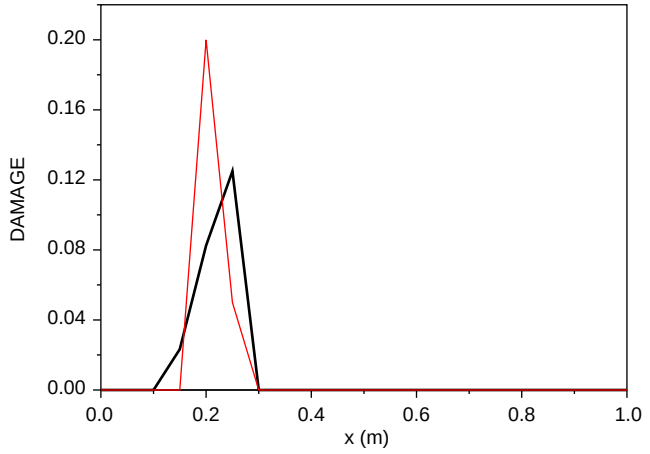

Fig. 11. Result obtained by *FCDIA* for case (4). Thin line: correct; thick line: obtained.

assumed to be measured, and only the cohesion parameters 2–9 were allowed to be updated. As the solution was restricted to a certain region, the regularization coefficient α was set to zero, in order to not penalize the gradient of furnished result. The authors have chosen to relocate the sensors to positions which encompass the indicated damaged region.

The result provided by *FCDIA* for the case (5) is graphed in Fig. 12. When analyzing the set of error measures associated with this case, depicted in Figs. 13–15, one may conclude that once again the updating process has furnished a positive result, corroborating the result obtained from the experiment in case (4). In reality, when comparing the errors measures, one may consider the result presented in Fig. 12 more accurate than that of Fig. 11, which is mainly disclosed for the relative frequency error E_f and the global time error *GTE*.

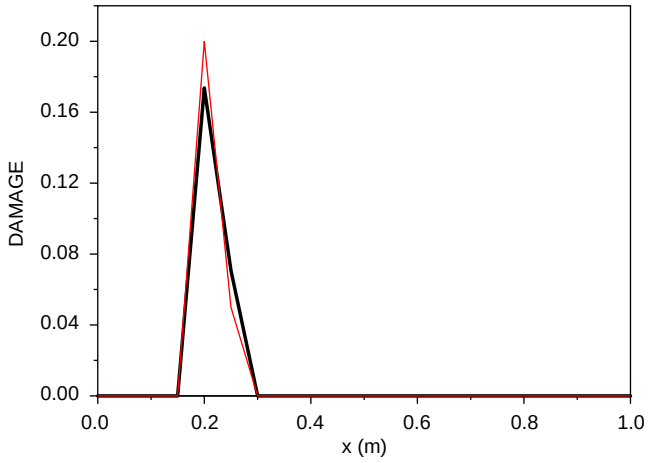

Fig. 12. Result obtained by *FCDIA* for case (5). Thin line: correct; thick line: obtained.

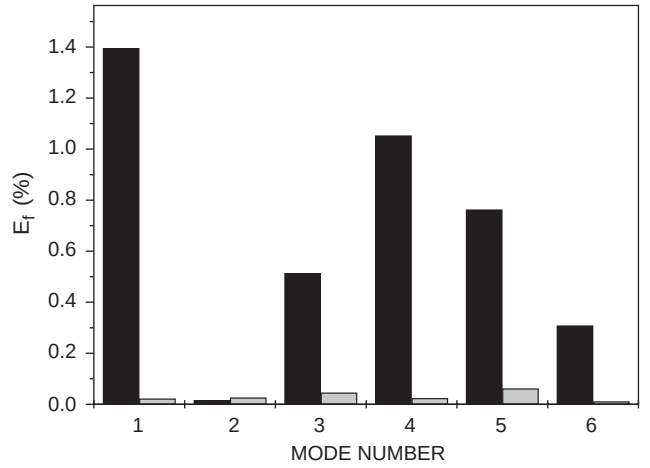

Fig. 13. Relative frequency error indicator E_f for case (5). Black columns: initial; gray columns: final.

The problem of damage identification in the presence of more severe noisy data is illustrated by case (6). In this case, the signal to noise ratio *SNR* has been set equal to 20 dB, which means that the rate of the variances of the signal and the noise attains 10%. In this case, for the data acquisition parameters as in Table 3, the result provided by *FCDIA* is graphed in Fig. 16.

As the results obtained for cases (6), (2) and (4) are very close, so are the errors indicators associated with these cases. Hence, all the error indicators, omitted here, are positive with respect to the provided result.

As it has already been mentioned, a new *FE* mesh for the damage field is introduced. It is more refined than that of the displacement field; more precisely, the new finite element mesh parameter's size is half of the displacement one. So, case (7) considers an imposed damage

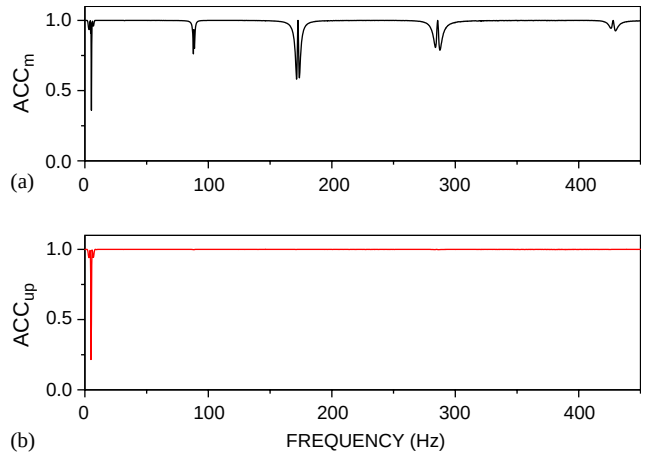

Fig. 14. Amplitude Correlation Coefficient ACC for case (5). (a) ACC_m: original model; (b) ACC_{up}: updated model.

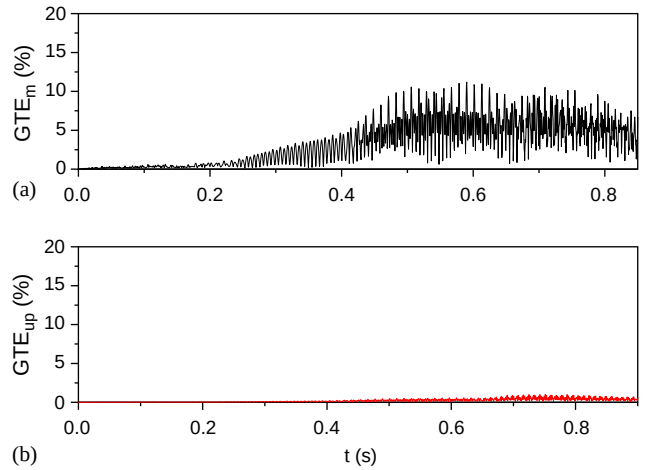

Fig. 15. Normalized global time error GTE for case (5). (a) GTE_m: original model; (b) GTE_{up}: updated model.

completely enclosed within the fourth element of the former mesh, and it is a linear distribution defined by the cohesion parameter $\beta = 0.6$ at a node in the middle of this element (0.175 m). It is assumed that every other vertical DOF has been measured, that $SNR = 90$ dB and that all the 42 cohesion parameters were allowed to be updated. The result obtained by $FCDIA$ and its associated error measures are shown in Fig. 17.

As it can be noted from Fig. 17, the result presented by $FCDIA$ was capable of satisfactorily indicating the damaged region, although its magnitude was not captured as well. However, the error measures, Figs. 18–20, are all very positive with respect to the provided result.

Case (8) deals with the same damage region as previously except that the measured DOFs are the vertical ones of the nodes 2, 6, 10, 14 and 18. The SNR for this case has been set equal to

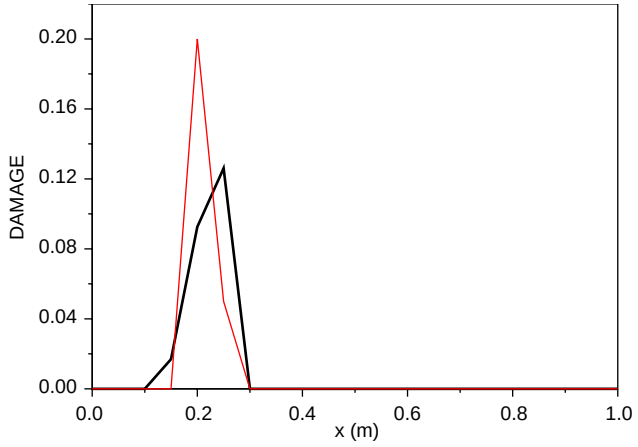

Fig. 16. Result obtained by *FCDIA* for the case (6). Thin line: correct; thick line: obtained.

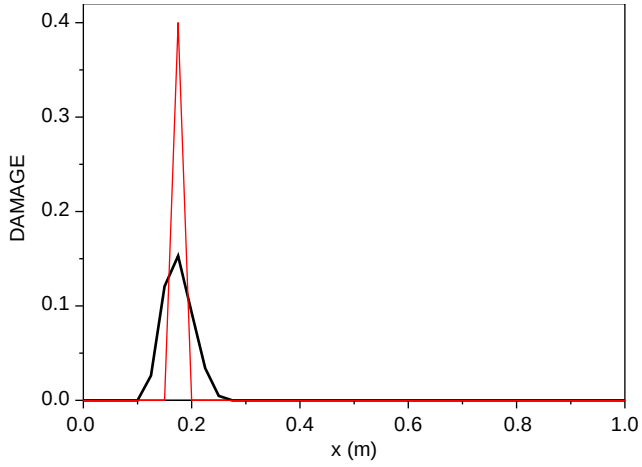

Fig. 17. Result obtained by *FCDIA* for case (7). Thin line: correct; thick line: obtained.

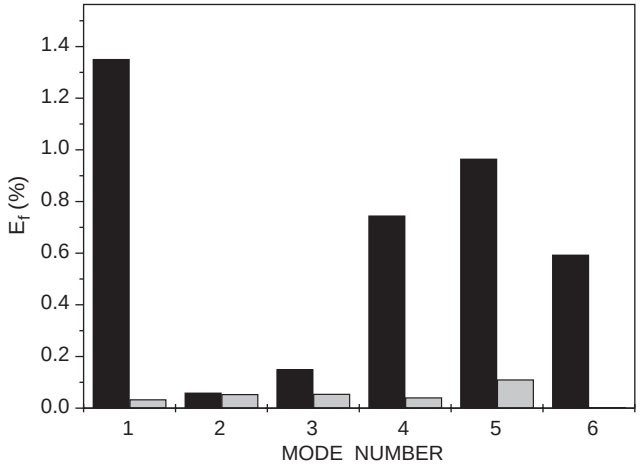

Fig. 18. Relative frequency error indicator E_f for case (7). Black columns: initial; gray columns: final.

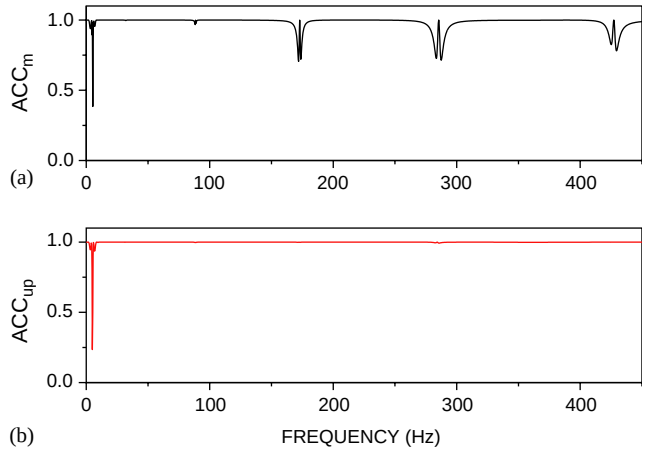

Fig. 19. Amplitude Correlation Coefficient ACC for case (7). (a) ACC_m: original model; (b) ACC_{up}: updated model.

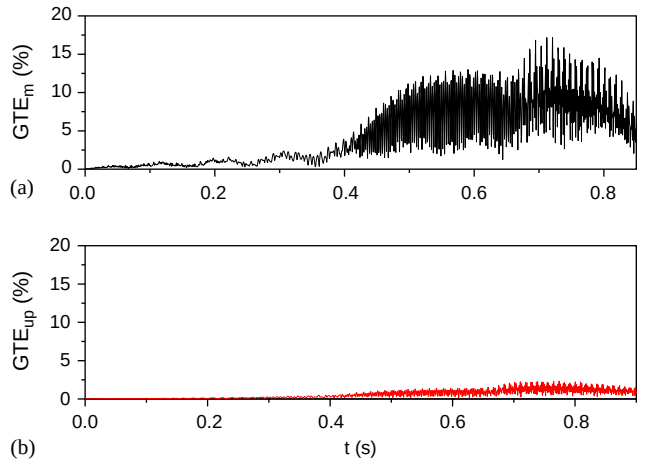

Fig. 20. Normalized global time error GTE for case (7). (a) GTE_m: original model; (b) GTE_{up}: updated model.

20 dB. The result obtained by *FCDIA* is depicted in Fig. 21; As one can see from Fig. 21, the damage identification result does not represent with fidelity the real damage present in the structure. Nevertheless, all the error measures, Figs. 22–24, are positive with respect to the provided result, which implies that the present result could be considered an improvement of the finite element model.

Cases (9)–(11) consider, once again, the feasibility of carrying out a second experiment on the same structure. As it has been done in case (5), the sensors were relocated to positions chosen based on the result provided by Fig. 21; see Table 3. In case (9), all the cohesion parameters were allowed to be updated. In cases (10) and (11), only a subset of the cohesion parameters pinpointed in Fig. 21 were allowed to be updated and the regularization coefficient α was set equal to zero. The results for cases (9) and (10) are depicted in Figs. 25 and 26, respectively.

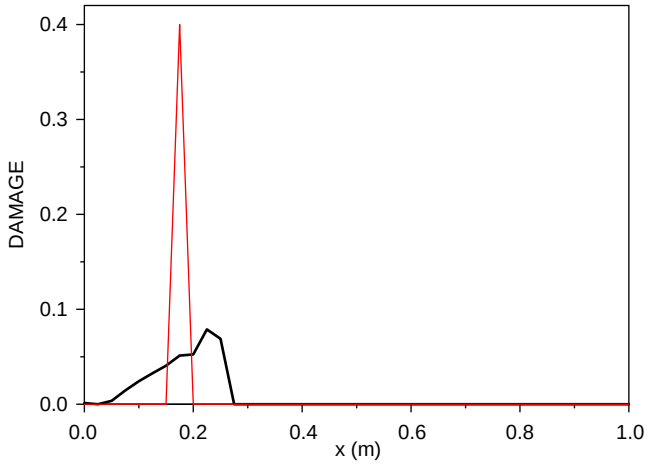

Fig. 21. Result obtained by *FCDIA* for case (8). Thin line: correct; thick line: obtained.

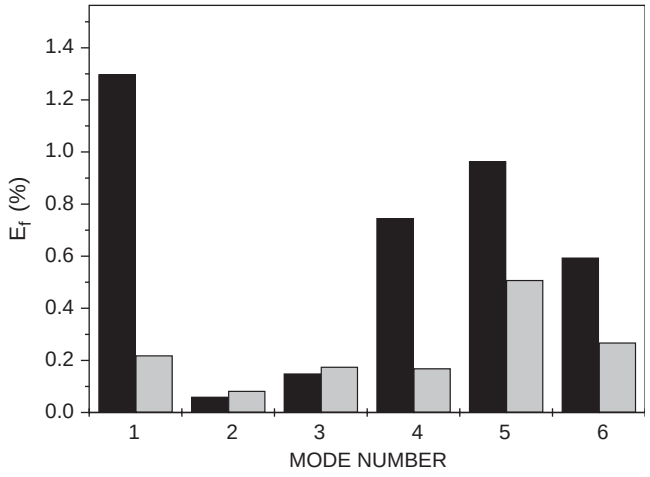

Fig. 22. Relative frequency error indicator E_f for case (8). Black columns: initial; gray columns: final.

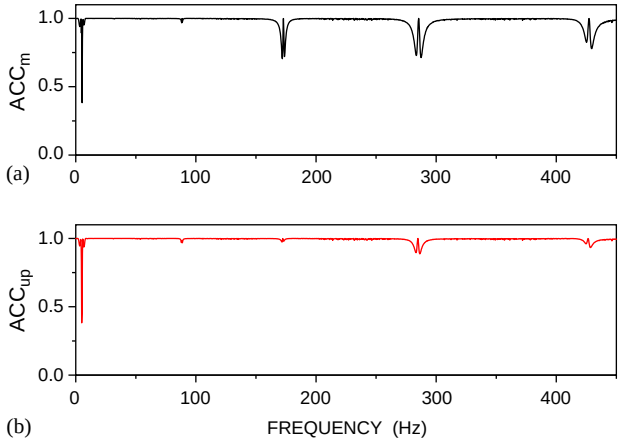

Fig. 23. Amplitude Correlation Coefficient ACC for case (8). (a) ACC_m: original model; (b) ACC_{up}: updated model.

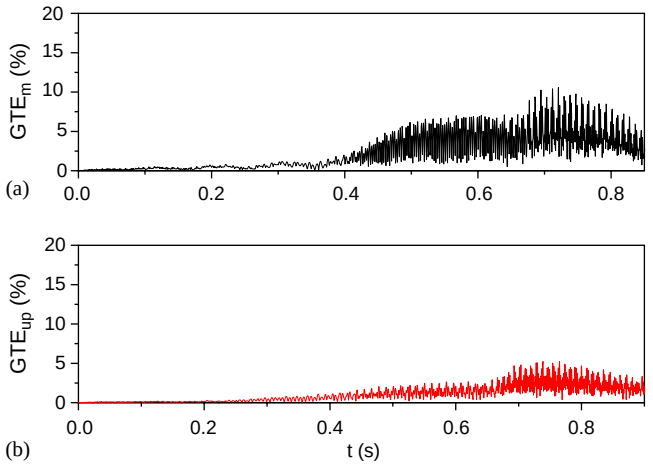

Fig. 24. Normalized global time error *GTE* for case (8). (a) GTE_m: original model; (b) GTE_{up}: updated model.

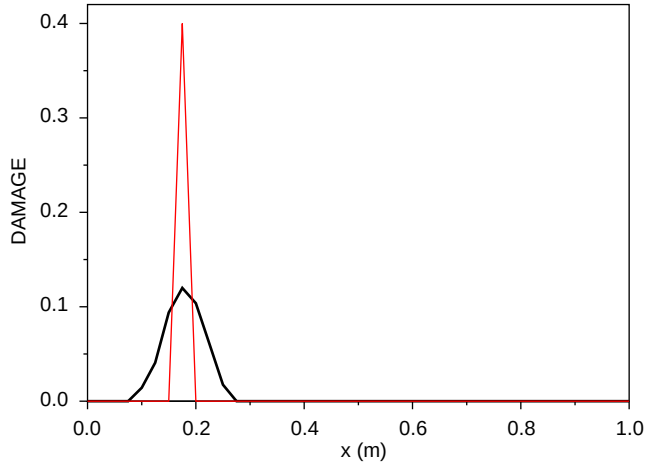

Fig. 25. Result provided by *FCDIA* for case (9). Thin line: correct; thick line: obtained.

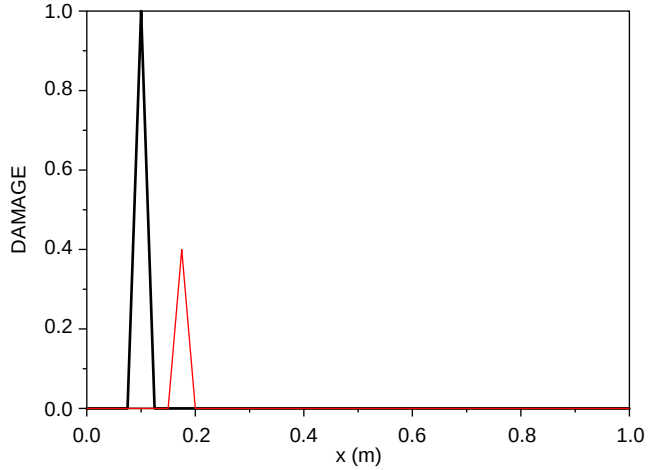

Fig. 26. Result provided by *FCDIA* for case (10). Thin line: correct; thick line: obtained.

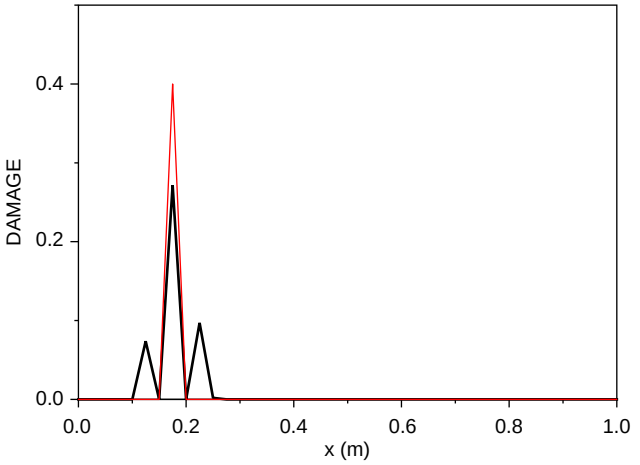

Fig. 27. Result provided by *FCDIA* for case (11). Thin line: correct; thick line: obtained.

The result provided by *FCDIA* in case (9) is a satisfactory one, however the result in case (10) represents an inconsistent one, inasmuch as it indicates a rupture of the beam at $0.1m$, corresponding to node 4 of the cohesion parameter mesh. Here once again one has an indication of the applicability of the regularization factor inasmuch as it has been set equal to zero for case (10).

As a last check, case (11) is almost equal to case (10) but only the cohesion parameters 5–11 were allowed to be updated. Although the present result can satisfactorily capture the amplitude of the imposed damage, as disclosed in Fig. 27, two other close small damaged regions are indicated. Nevertheless the results in cases (9) and (11) are distinct; the error measures associated with them, not depicted here, are very close.

5.1. *Preliminary assessment of the influence of parameter uncertainties*

A preliminary assessment of the parameter uncertainties influence in *FCDIA* is now presented. Several examples leading to similar conclusions were carried out considering Young modulus E variability along the structure and submitted to the same conditions of case (7), summarized in Table 3. The results depicted in Fig. 28 considers a 3% variation of the elastic parameter. They reveal that, despite the presence of the parameter uncertainty, the damaged region was indicated by *FCDIA*. As one can note from Fig. 29, the relative frequency error E_f shows the relative improvement of the updated model. It is worthwhile noting that the result presented in Fig. 28 indicates, in some sense, the presence of parameter uncertainties since damage is considered as a local phenomenon and a damage field distributed over the entire structure was obtained.

6. Concluding remarks

An approach for detecting damage based on a continuum damage model and using partial experimental modal parameters has been presented. It is built on a constrained minimization of a

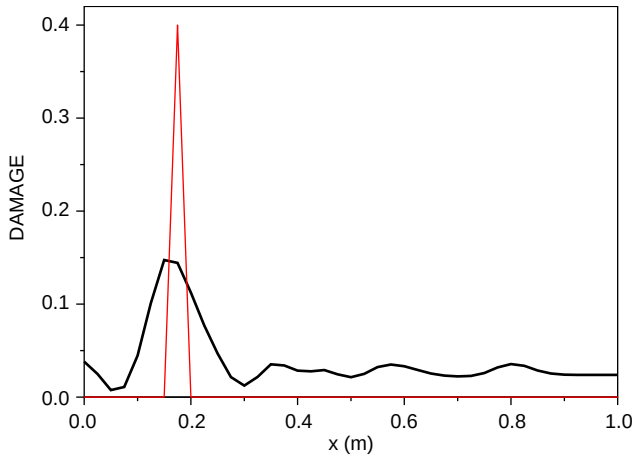

Fig. 28. Result provided by *FCDIA*. Thin line: correct; thick line: obtained.

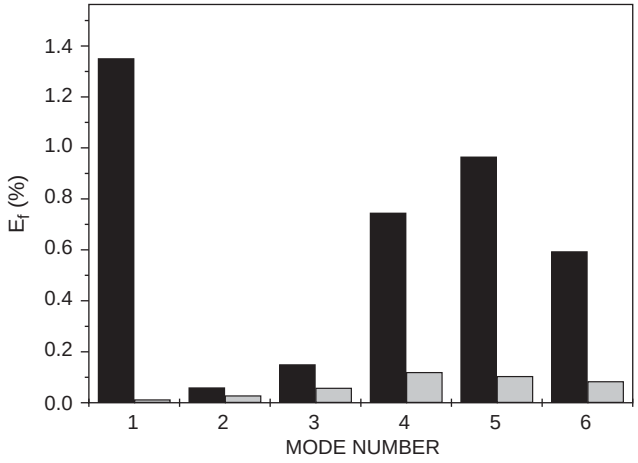

Fig. 29. Relative frequency error indicator E_f. Black columns: initial; gray columns: final.

least-square residue involving model and experimental flexibility matrices. The approach has been assessed using a number of different examples. The simulations have been performed on situations involving typical real shortcomings, where the corrupting effects of noise, filtering, digital sampling, truncation of the modal spectrum and the limited number of sensors have been considered. The eigensystem realization algorithm (*ERA*) along with the common-based normalized system identification (*CBSI*) were utilized to obtain the required natural frequencies and mode-shapes.

The method has been shown to be efficient for estimating damage scenarios for the presented situations. The validity of the provided results was based on a set of error measures. This set of error measures is capable of qualifying whether a result is coherent or not, nevertheless, it has not been shown to be a straightforward measure in comparing different results for the same problem.

The efficiency of the present approach depends upon the *FE* model accuracy, which, in practice, is affected by the unavoidable presence of uncertainties. They exist due to inaccurate physical parameters, non-ideal boundary conditions, localized non-linear behavior, discretization errors and noise measurements. The *FCDIA* copes with those shortcomings by adopting a two stage model updating. The first stage involves the updating of the undamaged structure, in order to handle some of the mentioned sources of uncertainties. The authors have reported their own experience involving the updating of composites structures in Refs. [33–35]. The second stage consists of damage identification considering only noise measurements as uncertainties. Their impact along with the variability of physical properties on *FCDIA* is preliminarily addressed in the previous chapter. Further efforts in order to deal with uncertainties in the context of the proposed method are now in progress.

Finally, it is important to reinforce that in the author's experience a significative way of improving the performance of any damage identification approach relies on the developing of reliable error indicators, which could help in evaluating the quality of the estimated damage. They can work on an adaptive strategy, like those traditionally used in the finite element technology, verifying whether the damage identification was successful and, if it was not, indicating ways of improving it. Remeshing and sensors relocation would be two possible actions in that context.

References

[1] S.W. Doebling, C.R. Farrar, M.B. Prime, D.W. Sheritz, 1996 *Los Alamos National Lab.*, Rept. LA-13070-MS, Los Alamos. Damage Identification and Health Monitoring of Structural and Mechanical Systems from Changes in their Vibration Characteristics: A Literature Review.

[2] J.E. Mottershead, M.I. Friswell, Model updating in structural dynamics, *Journal of Sound and Vibration* 167 (2) (1993) 347–375.

[3] Y. Zou, G.P. Steven, Vibration-based model-dependent damage (delamination) identification and health monitoring for composite structures—a review, *Journal of Sound and Vibration* 230 (2) (2000) 357–378.

[4] J.H. Chou, J. Ghaboussi, Genetic algorithm in structural damage detection, *Computers & Structures* 79 (14) (2001) 1335–1353.

[5] N. Hu, X. Wang, H. Fukunaga, Z.H. Yao, H.X. Zhang, Z.S. Wu, Damage assessment of structures using modal test data, *International Journal of Solids and Structures* 38 (18) (2001) 3111–3126.

[6] M. Kaouk, D.C. Zimmerman, Structural damage assessment using a generalized minimum rank perturbation theory, *AIAA Journal* 32 (4) (1994) 836–842.

[7] H.T. Banks, D.J. Inman, D.J. Leo, Y. Wang, An experimentally validated damage detection theory in smart structures, *Journal of Sound and Vibration* 191 (5) (1996) 859–880.

[8] D.A. Castello, L.T. Stutz, F.A. Rochinha, A time domain technique for defect identification based on a continuum damage model, *Proceedings of the 2002 ASME International Mechanical Engineering Congress & Exposition*, November 17–22, New Orleans, Louisiana, USA, 2002.

[9] A. Pandey, M. Biswas, Damage detection in structures using changes in flexibility, *Journal of Sound Vibration* 169 (1) (1994) 3–17.

[10] M. Baruch, Optimal correction of mass and stiffiness matrices using measured modes, *AIAA Journal* 20 (11) (1982) 1623–1626.

[11] A.M. Kabe, Stiffness matrix adjustment using mode data, *AIAA Journal* 23 (9) (1985) 1431–1436.

[12] C. Farhat, F.M. Hemez, Updating finite element dynamic models using an element-by-element sensitivity methodology, *AIAA Journal* 31 (9) (1993) 1702–1711.

[13] D.A. Castello, L.T. Stutz, F.A. Rochinha, A structural defect identification based on a continuum damage model, *Computers & Structures* 80 (5–6) (2002) 417–436.

[14] T.W. Lim, T.A.-L. Kashangaki, Structural damage detection of space truss structures using best achievable eigenvector, *AIAA Journal* 32 (5) (1994) 1049–1057.
[15] D.C. Zimmerman, W. Widengren, Correcting finite-element models using a symmetrical eigenstructure assignment technique, *AIAA Journal* 28 (9) (1990) 1670–1676.
[16] S.M. Pires-Domingues, H.S.C. Mattos, F.A. Rochinha, Modelling of nonlinear damage on elastic brittle materials, *Mechanics Research Communications* 25 (2) (1998) 147–153.
[17] L.T. Stutz, Damage identification approach via flexibility matrix adjustment based on a continuum damage model, M.Sc. Dissertation, Federal University of Rio de Janeiro, Brasil, 1999 (in Portuguese).
[18] K.K. Denoyer, L.D. Peterson, Model update using modal contribution to static flexibility error, *AIAA Journal* 35 (11) (1997) 1739–1745.
[19] S.W. Doebling, L.D. Peterson, K.F. Alvin, Estimation of reciprocal residual flexibility from experimental modal data, *AIAA Journal* 34 (8) (1996) 1678–1685.
[20] B. Titurus, M.I. Friswell, J.E. Mottershead, Damage detection using general elements: Part II. damage detection, *Computers & Structures* 81 (2003) 2287–2299.
[21] B. Titurus, M.I. Friswell, J.E. Mottershead, Damage diagnosis using time series analyis of vibration signals, *Smart Materials and Structures* 10 (2001) 1–6.
[22] F.M. Hemez, S.W. Doebling, Review and assessment of model updating for non-linear, transient dynamics, *Mechanical Systems and Signal Processing* 15 (1) (2001) 45–74.
[23] H. Ahmadian, J.E. Mottershead, M.I. Friswell, Regularisation methods for finite element model updating, *Mechanical Systems and Signal Processing* 12 (1) (1998) 47–64.
[24] H.W. Park, S. Shin, H.S. Lee, Determination of an optimal regularization factor in system identification with tikhonov regularization for linear elastic continua, *International Journal for Numerical Methods in Engineering* 51 (10) (2001) 1211–1230.
[25] K.F. Alvin, L.D. Peterson, K.C. Park, Method for determining minimum-order mass and stiffness matrices from modal test data, *AIAA Journal* 33 (1) (1995) 128–135.
[26] R.J. Guyan, Reduction of stiffness and mass matrices, *AIAA Journal* 3 (2) (1965) 380.
[27] J. Skrzypek, A. Ganczarski, *Modeling of Material Damage and Failure of Structures: Theory and Applications*, Springer, Berlin, 1999.
[28] H.S.C. Mattos, R. Sampaio, Analysis of the fracture of brittle elastic materials using a continuum damage model, *Structural Engineering and Mechanics* 3 (5) (1995) 411–427.
[29] J.M. Ricles, J.B. Kosmatka, Damage detection in elastic structures using vibratory residual forces and weighted sensitivity, *AIAA Journal* 30 (9) (1992) 2310–2316.
[30] J.N. Juang, R.S. Pappa, An eigensystem realization algorithm for modal parameter identification and model reduction, *Journal of Guidance, Control and Dynamics* 8 (5) (1985) 620–627.
[31] K.F. Alvin, K.C. Park, A second order structure identification procedure via state space-based system identification, *AIAA Journal* 32 (2) (1994) 397–406.
[32] H. Grafe, Model updating of large structural dynamics models using measured response functions, 1998 Ph.D. Thesis, Imperial College of Science, Technology and Medicine University of London, 1998.
[33] S.F. Bastos, L. Borges, F.A. Rochinha, Numerical and experimental approach for identifying elastic parameters in sandwich plates, *Shock and Vibration* 9 (4–5) (2002) 193–201.
[34] D.A. Castello, F.A. Rochinha, An experimental assessment of transverse adaptive filters as applied to vibrating structures identification, *Shock and Vibration in July, 2003*, submitted.
[35] R.R.F.O. Pereira, D.A. Castello, F.A. Rochinha, A time domain based mechanical system identification, 17th *International Congress of Mechanical Engineering* (*COBEM 2003*), São Paulo, S.P., Brazil, November 10–14, 2003.